Photon energy dependent circular dichroism in angle-resolved photoemission from Au(111) surface states

Hanyoung Ryu,[1,2] Inkyung Song,[1,2] Beomyoung Kim,[3,4] Soohyun Cho,[2,5] Shoresh Soltani,[2,5] Timur Kim,[6] Moritz Hoesch,[6] Choong H. Kim,[1,2] and Changyoung Kim[1,2,*]

[1]*Department of Physics and Astronomy, Seoul National University (SNU), Seoul 08826, Republic of Korea*
[2]*Center for Correlated Electron Systems, Institute for Basic Science (IBS), Seoul 08826, Republic of Korea*
[3]*Advanced Light Source, Lawrence Berkeley National Laboratory, Berkeley, California 94720, USA*
[4]*Department of Physics, Pohang University of Science and Technology, Pohang 790-784, Korea*
[5]*Institute of Physics and Applied Physics, Yonsei University, Seoul 120-749, Korea*
[6]*Diamond Light Source, Harwell Campus, Didcot OX11 0DE, United Kingdom*

(Received 21 December 2016; revised manuscript received 9 February 2017; published 24 March 2017)

We performed angle-resolved photoemission experiments on Au(111) surface with circularly polarized light. Data were taken with photon energies in the range between 20 and 100 eV in order to investigate the photon energy dependent behavior in the circular dichroism (CD). While the magnitude of the normalized CD value varies with a maximum value of about 70%, the sign of CD does not change for the photon energy within the range, inconsistent with the prediction based on the density-functional theory (DFT) calculation. Our calculation of the CD using DFT initial state and free electron final state shows a better consistency with experimental results than an earlier study using the inverse low-energy electron diffraction state as the final state. We briefly discuss the dominating factor that determines the CD from Au(111) states.

DOI: 10.1103/PhysRevB.95.115144

I. INTRODUCTION

Circular dichoism (CD) in angle-resolved spectroscopy (ARPES) was observed in spatially oriented carbon monoxide molecules on Pd(111) [1]. Since then, CD-ARPES has been used to investigate various aspects of the electronic structures of materials. For example, it was proposed, based on the CD-ARPES data, that time-reversal symmetry is broken in the pseudogap states of cuprate superconductors [2,3]. In addition, data from graphene suggests that CD-ARPES may be used as a tool to investigate the phase information of the wave function [4]. Recently, much attention has been paid to CD-ARPES on spin-split states. CD-ARPES studies have been performed on topological insulators (TIs) [5–7] as well as systems with Rashba-type spin split surface states such as Au(111), Cu(111) [8], and Bi/Ag(111) [9].

There have been various proposals on what the dominating factor of the CD is, including spin [5], orbital angular momentum (OAM) [7,10], and the phase of wave function [4] of the initial state as well as the experimental geometry [11]. In addition, it was argued that the final-state effect should be considered to interpret experimental data properly [12,13], based on the photon energy dependent data in which even the sign of the CD-ARPES changes as the incident photon energy varies [12–16]. As a result, the origin of the dichroic signal in CD-ARPES is still under debate. However, since the photoemission transition rate involves both the initial and final states, the question is if one of them dominantly determines CD-ARPES.

The Au(111) surface state is one of the most studied Rashba-type spin split bands [17]. Chiral spin structure in the surface state was confirmed both theoretically [18] and experimentally [19]. In addition to the spin structure, chiral OAM structure has been shown to exist in the state [8]. In this respect, the Au(111) surface state is a model system to study the issue including the role of the final states in CD-ARPES. Indeed, calculated photon energy dependent CD-ARPES has been recently reported [16]. The results appear to be quite different from published experimental CD-ARPES taken with a 10-eV photon [8]. However, the differences in the photon energy and incident angle do not allow us a fair comparison between the theory and experiment.

As the comparison between the theory and experiment is essential in elucidating the dominant cause of the CD signal, it is also important to have systematic photon energy dependent experimental CD-ARPES data on Au(111) surface states. Therefore, we performed a CD-ARPES experiment on the Au(111) surface state with a wide range of photon energies, from 20 to 100 eV. Our experimental result clearly shows features that depend on the photon energy. Our results show a rather simple $\sin\theta$ form for most of the photon energies we used [see Fig. 2(a) for the definition of the azimuthal angle θ] [6,8]. The lack of a complex CD pattern is inconsistent with the published calculation results [16]. Our systematic data should be useful for further investigation on the photoemission process involving spin split bands such as Au(111) states.

II. METHODS

ARPES experiments were performed at the beam line I05 of the Diamond Light Source equipped with the VG-Scienta R4000 electron analyzer. The Au(111) single crystalline sample was prepared by repetitive Ar sputtering and annealing at a 700-K process to obtain a clean surface condition. Data were taken at 12 K in a vacuum better than 1.2×10^{-10} mbar with right and left circularly polarized (RCP and LCP, respectively) light. Photon energies used in the experiments were between 20 and 40 eV with a 1-eV energy step and

*changyoung@snu.ac.kr

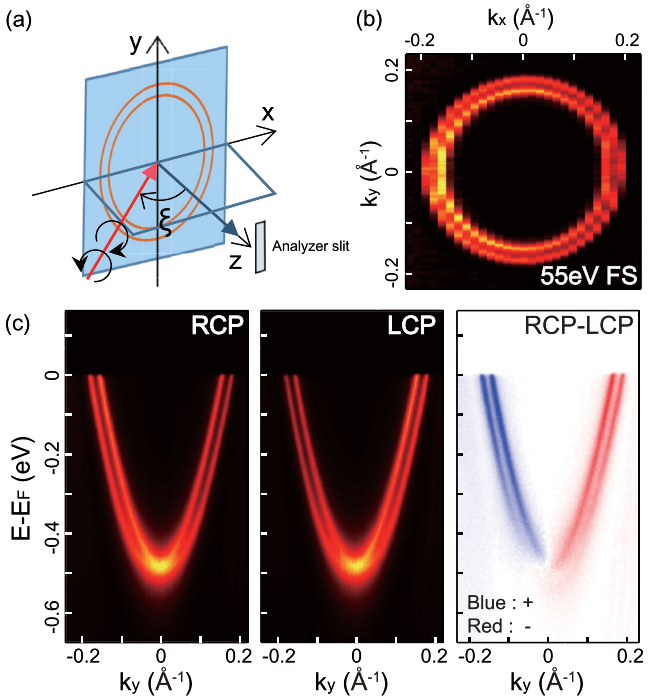

FIG. 1. (a) Experimental geometry and schematic Fermi surfaces of Au(111) surface states. Au(111) surfaces are in the xy plane. Angle between sample normal direction ($\hat{z}$) and incident photon ξ is 50° in this work. (b) Fermi surface (FS) data taken with 55-eV photon. (c) From left, RCP, LCP, and RCP-LCP data along the $k_x = 0$, taken with 21-eV photon, respectively.

43–100 eV with a 3-eV energy step. Circularly polarized light was injected into the sample from the positive k_x to negative k_x direction with 50° from the sample normal direction in the xz plane as depicted in Fig. 1(a).

We model Au(111) surfaces with a supercell including a slab of 24-layer and 15-Å thickness vacuum region. For density functional theory calculations within the local-density approximation, we employed the linear combination of pseudoatomic orbitals (LCPAO) method as implemented in OpenMX [20,21]. Spin-orbit interaction was included via the norm-conserving, fully relativistic j-dependent pseudopotential scheme in the noncollinear DFT formalism. To simulate the circular dichroism in ARPES, we take a plane wave for the final-state wave function $\psi_F(\boldsymbol{r}) \sim e^{i\boldsymbol{k}_F \cdot \boldsymbol{r}}$ where $\boldsymbol{k}_F$ is the wave vector of the final-state photoelectron. Then, the transition amplitude to the final state with spin σ is given by the overlap integral

$$I \sim \langle \psi_F | \boldsymbol{p} \cdot \boldsymbol{A} | \psi_I \rangle \sim \langle \psi_F | \boldsymbol{r} \cdot \boldsymbol{A} | \psi_I \rangle \quad (1)$$

within the dipole approximation. In our calculation, we consider only the dipole transition term and ignore the other terms such as relativistic correction which is considered in other studies [5,9,16]. The in-plane component of k_F matches the momentum of the band electron (initial state) and the z component of the final-state momentum is fixed as $k_F^z = 2.27\ \text{Å}^{-1}$ consistent with the photoelectron energy in the actual experiment described in Ref. [8].

III. RESULTS AND DISCUSSION

A. Experimental result

Fermi-surface data taken with a 55-eV photon, displayed in Fig. 1(b), shows clear separation between the inner and outer Rashba-type spin split bands. The energy versus momentum (along the k_y direction) curve taken with RCP and LCP and their difference CD = RCP − LCP are plotted in Fig. 1(c). One can see the RCP (LCP) data have higher intensity in the $k_y < 0$ ($k_y > 0$) region. Such polarization dependent behavior is seen in the CD data, with red meaning negative and blue meaning positive. At the Γ point where bands are degenerate and neither spin nor OAM exists, there is no circular dichroic signal as expected. The binding energy at the Γ point is 480 meV and the Fermi momentum (k_F) are found to be 0.176 and $0.154\%^{-1}$ for outer and inner bands, respectively. The band dispersion as well as the CD behavior are consistent with published results [8,17,22].

CD data taken with various photon energies are shown in Fig. 2. Left panels show CD structure at 20 meV binding energy while the right panels are the energy-momentum distribution along the dashed line in the left panels, $k_x = 0$. There is a weak CD signal in the background away from the Rashba bands as seen in Fig. 2, but it is not of our interest and we will limit our discussion to the CD in the Rashba bands. We see that the CD has the same sign for the inner and outer bands. This same color behavior is consistently seen for most of the photon energies we used in the experiments. As the spin has opposite chiralities between the two Rashba bands [19,23], our observation is inconsistent with the interpretation that the CD data are representative of the spin texture [5]. Instead, the result is consistent with previous CD-ARPES work in which the CD is attributed to chiral OAM structure which has the same chirality for the inner and outer bands [8].

Paying attention to the CD pattern, we may note two aspects of the data. The left panels of the figure show that all of 29, 40, 55, and 82-eV 20-meV binding energy CD data have a simple sinθ form. However, in Fig. 5 of Ref. [16], the CD pattern is neither sinθ-like nor photon energy independent. CD calculation results change rapidly as the photon energy varies between 10 and 100 eV. For a direct comparison between theory and experiment, we discuss the calculated 30-, 40-, 55-, and 80-eV data in Ref. [16] in comparison with our experimental data. In calculated 30-eV data, the outer Rashba band shows a mostly positive CD value. On the other hand, a sinθ form CD is seen about a tilted line from k_x for the inner Rashba band. In 40-eV photon energy calculation data, both inner and outer bands show the same sign but a clear threefold symmetry is seen in the CD signal, inconsistent with our experimental result. As seen in Fig. 2 of our work, symmetric axes of all experimental data are k_x axis. The lack of a complex pattern in our experimental data is clearly inconsistent with the calculated result [16] and persists for other photon energies. The other aspect is that the pattern is fairly photon energy independent, which is also inconsistent with the calculation. Overall, the experimental data show simple and photon energy independent patterns.

To look at the photon energy dependence more closely, we plot the averaged NCD (ANCD), defined as the mean

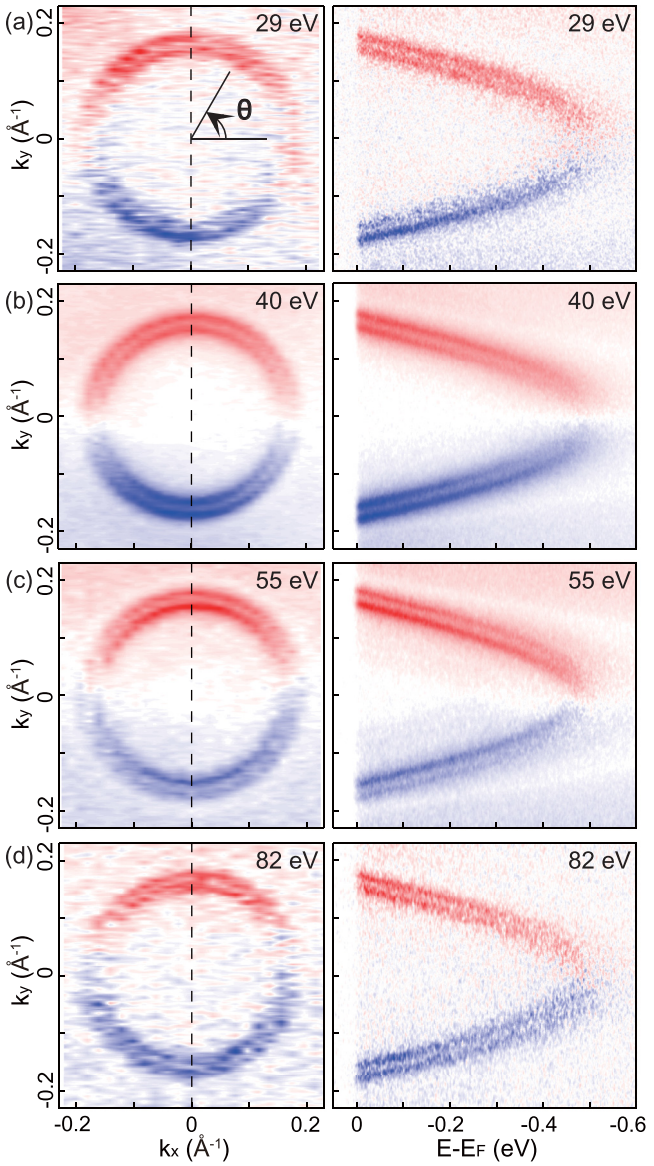

FIG. 2. Left panels of (a)–(d) are RCP-LCP mapping data at 20 meV binding energy measured with photon energy 29, 40, 55, and 82 eV, respectively. Right panels are RCP-LCP cut data along the $k_x = 0$ cut (dashed line in left panels).

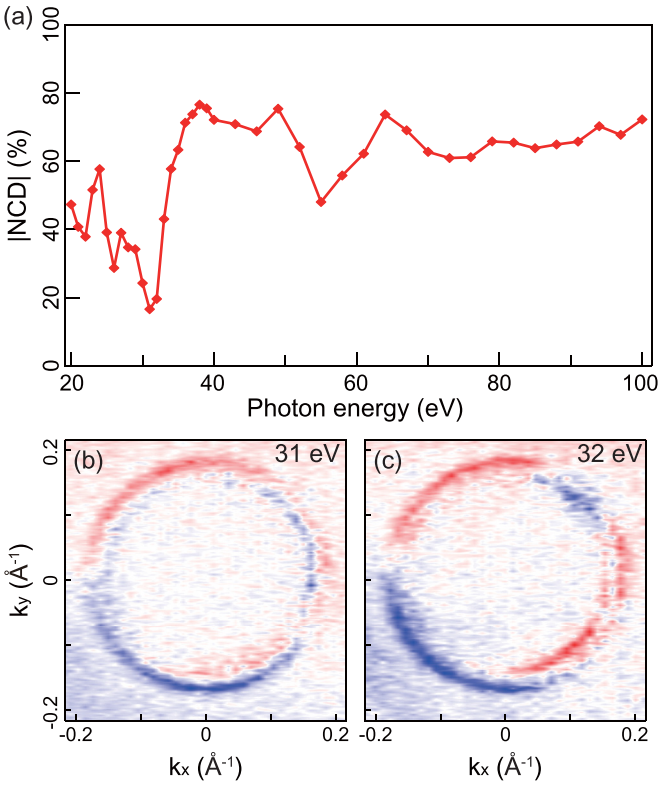

FIG. 3. (a) Averaged normalized CD (NCD) at $(k_x,k_y) = (0,k_F^{\text{out}})$ and $(0,k_F^{\text{in}})$ points taken with photon energy from 20 to 100 eV. (b),(c) Constant energy CD map at 20 meV binding energy taken with 31 and 32 eV photon, respectively.

of the values at $(k_x,k_y) = (0,k_F^{\text{out}} > 0)$ [i.e., $(0,0.176\,\text{Å}^{-1})$] and $(0,k_F^{\text{in}} > 0)$ [i.e., $(0,0.154\,\text{Å}^{-1})$], as a function of all photon energies in Fig. 3(a). From 20 to 31 eV, the overall ANCD value decreases as the photon energy increases with a minimum NCD value of 17% at 31 eV. The ANCD value shows a drastic increase as the photon energy changes from 31 to 38 eV, reaching 77%. Above 38 eV, the ANCD value shows relatively little change, staying between 75% (at 39 eV) and 61% (at 73 eV) except the region around 55 eV. In addition, the CD pattern remains more or less the same with a $\sin\theta$ form as mentioned above. The little effect of the photon energy on the CD-ARPES suggests that the final-state effect is relatively weak for the Au(111) surface state, at least for photon energies above 40 eV. This casts a sharp contrast to the Bi_2Se_3 and Bi_2Te_3 cases where a strong photon energy dependence has been observed [12,13].

While the photon energy dependence is not strong in general, there is a dip in the ANCD curve at around 31 eV photon energy. The CD patterns at 20 meV binding energy for 31 and 32 eV photons are shown in Fig. 3(b) and 3(c), respectively. At these two photon energies, we do not see the simple $\sin\theta$ form in the CD structure seen at other photon energies. In the 31-eV data, the CD value of the inner band is mostly positive (negative) in $k_y > 0$ ($k_y < 0$) region. Meanwhile, the 32-eV data show a peculiar pattern on both outer and inner bands. These are clearly different from behavior of the data taken with other photon energies. As the initial states stay the same, such behavior must come from the character of the final state discussed in the case of Bi_2Se_3 and Bi_2Te_3 [12,13]. On the other hand, we also note that the abnormal CD pattern with the lowest NCD value observed around 31 eV accompanies the lowest total intensity, RCP + LCP (not shown in this paper). Variation in the cross section for noble-metal surfaces including Au(111) has been reported [24–26]. This implies that the usual transition channel that gives the simple $\sin\theta$ form in CD is somehow suppressed around 31 eV. Then, other effects may become important and bring about the complex CD pattern.

B. Calculation

In order to elucidate the issues raised above, we performed DFT calculation on Au(111) surface states. Plotted in Fig. 4 is

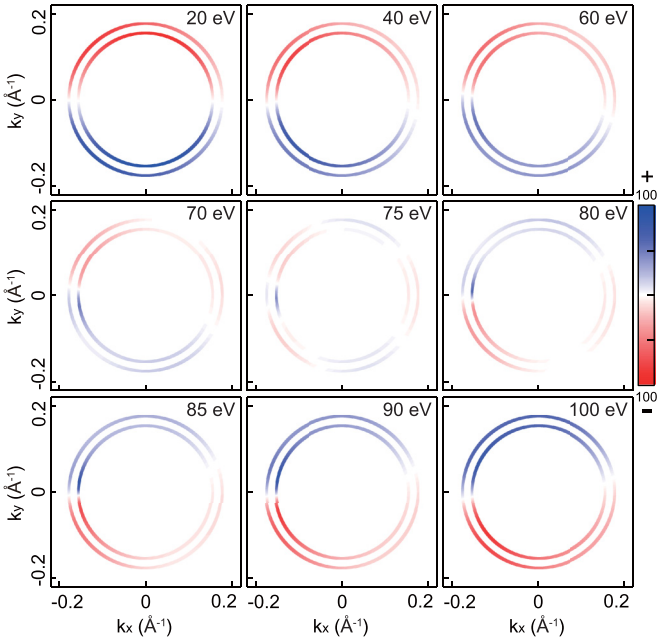

FIG. 4. DFT calculation in 20–100 eV photon energy with 45° incident photon. The outer band wave vector (k_F^{out}) is 0.176 $\%^{-1}$ and inner band wave vector (k_F^{in}) is 0.154 $\%^{-1}$.

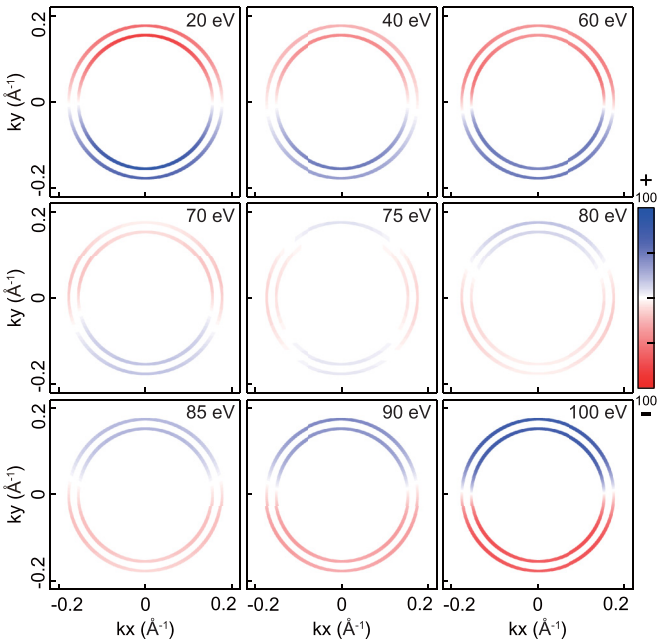

FIG. 5. Calculated CD-ARPES for grazing incident ($\xi = 90°$) photons in 20–100-eV range. The CD signal in the grazing incident case represents in-plane OAM contribution.

the calculation of the photon energy dependent Fermi-surface NCD of the Au(111) surface state. We used the free-electron wave function as the final state along with the DFT initial state in the calculation. The photon energy ranges from 20 to 100 eV as is the case for the experiment. The photon incident angle was taken to be 45° which is similar to the experimental incidence angle, 50°. In the low-energy region, 20–70 eV, the calculation shows a simple form of sinθ and the same CD sign for the two bands. This is consistent with the experimental data. However, as the photon energy reaches 70 eV, the pattern begins to change to a more complex pattern. When the photon energy is above 85 eV, the CD pattern recovers the sinθ pattern but with the sign reversed. Note that the sign of the CD is almost always the same for the inner and outer bands, even when the pattern gets quite complicated for the photon energy between 70 and 85 eV. This fact that CD shows the same sign for the inner and outer bands solidifies the notion that CD-ARPES is sensitive to the OAM texture, not the spin [8].

Comparing our calculation with the published one [16] which is based on fully relativistic calculation (for example, Fig. 5 in the reference), we find a quite different tendency in the CD pattern. In our DFT result, the CD pattern shows mostly a simple sinθ form about the k_x axis in 20–100-eV photon energy except the region around 75 eV where there is a sign change. On the contrary, the data in Ref. [16] show a rather complex pattern. In addition, the CD signals from the inner and outer bands have opposite signs for most of the photon energies. One may attribute the difference to the difference in the photon incident angle ($\xi = 45°$ for our case and 30° in Ref. [16]). However, OAM and spin textures of Au(111) surface states have a much larger in-plane component than out-of-plane component [8,22]. Therefore, the CD pattern should follow the in-plane OAM texture unless the incident angle is almost zero in which case the CD picks up only the out-of-plane component of the OAM [7]. An earlier angle dependent CD calculation also shows that the CD signal follows the in-plane OAM texture when the incident angle is above 10° [16]. These mean that the two calculation results in principle should be similar to each other. Therefore, it is rather peculiar to find the two calculation results quite different. It is interesting to note that the calculation done with a simpler method (ours) is more consistent with the experimental data than the fully relativistic calculation [16].

There is also a peculiar aspect in the photon energy dependence of the Fermi-surface CD pattern. At 75 eV in calculation and 31 and 32 eV in experiment, the CD structure does not have a simple sinθ structure. We note that the out-of-plane OAM has threefold symmetry due to the underlying crystal symmetry [22]. While the chiral in-plane OAM gives a sinθ form in the CD pattern, the threefold symmetry in the out-of-plane OAM results in a cos3θ form. For Au(111) surface states, the in-plane OAM component is much larger than the out-of-plane component [22]. Therefore, the CD signal is usually dominated by the in-plane OAM contribution rather than the out-of-plane contribution as mentioned above. However, the out-of-plane contribution may become comparable (or even dominant) and a complex pattern can appear if the in-plane contribution becomes weak for some photon energies due to the matrix element effect.

If the above scenario is right, the peculiar complex CD patterns should appear at photon energies where NCD is weak. To investigate the possible relationship between the weak in-plane contribution and the peculiar complex CD pattern, we calculated the CD-ARPES for grazing ($\xi = 90°$) and normal ($\xi = 0°$) incident cases. In this case, the grazing and normal incident cases represent the in-plane and out-of-plane OAM

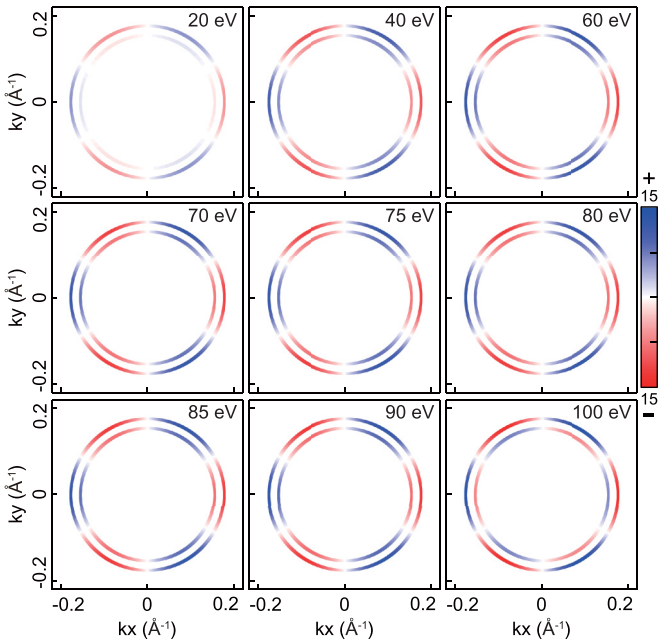

FIG. 6. Calculated CD-ARPES for normal incident ($\xi = 0^\circ$) photons in 20–100-eV range. CD taken with normal incident photons should show the out-of-plane OAM contribution. Note that the color scale used in this figure is not the same as those used in Figs. 4 and 5.

contributions, respectively [7]. The grazing incident case is plotted in Fig. 5. The CD signal shows a simple $\sin\theta$ structure without a complex pattern for all photon energies except 75 eV where CD sign is inverted. The fact that CD signal is relatively weak at 75 eV, ranging between -8.9% and 14.1%, suggests that the out-of-plane OAM component can contribute to the CD signal and a complex pattern may appear as seen in the 75-eV data in Fig. 4. The normal incident case which represents the out-of-plane OAM contribution is plotted in Fig. 6. Calculation results show a simple $\cos 3\theta$ form with less than 15% NCD values for all photon energies. The NCD value at 75 eV for the normal incident case, -12.3% to 12.3%, is comparable to that of the grazing incidence case, -8.9% to 14.1%. Therefore, we attribute the complex CD pattern at certain photon energies to the superposition of $\sin\theta$ and $\cos 3\theta$ structures from in-plane and out-of-plane contributions, respectively.

Even though there is a good overall agreement between our experimental and DFT calculation results, the experimental data do not show sign reversal in NCD within the photon energy range we used. One may suspect the use of free electron final state as the culprit for the difference as use of free electron states is more likely to suppress the final state variation compared to the real true states. However, we note that our calculation is more compatible with the experimental data than the calculation that incorporates the inverse low-energy electron-diffraction (inverse LEED) states. Therefore, use of free-electron states as approximate final states cannot explain the difference. The real culprit may come from the discontinuity of vector potential of the photon at the surface which was investigated for Ag and other metallic surfaces [9,27]. The discontinuity of vector potential at the surface induces a surface term which is proportional to $\nabla \cdot \mathbf{A}$ in the matrix element ($\mathbf{A}$ is the vector potential of the photon) but is not included in the calculations. This surface term may be an important factor in the photoemission process and thus the photon energy dependence.

IV. CONCLUSION

In this paper, we investigate the magnitude and pattern of Au(111) surface state CD-ARPES in a wide range of photon energies, both experimentally and theoretically. In most of the photon energies we used, a simple CD pattern with a $\sin\theta$ form is seen, as was in our previous work with a low photon energy [8]. In addition, the magnitude of the NCD value is fairly photon energy independent above a photon energy of 40 eV. These observations are inconsistent with earlier fully relativistic DFT calculation involving the final-state effect [16] but are more consistent with our DFT calculation with a free electron final state. The fact that CD shows the same sign for the inner and outer bands at all photon energies indicates that the CD signal is sensitive to the OAM information in the Au(111) surface states. Our study showing the same CD sign for inner and outer bands strengthens the possibility for CD-ARPES as a tool to study the existence and structure of OAM in the initial states.

ACKNOWLEDGMENTS

The work was supported by IBS-R009-G2. S.S. and S.C. acknowledge support from the Yonsei University BK21 program. The data presented in this paper were taken at beamline I05, Diamond Light Source, under Proposal No. SI11445.

[1] C. Westphal, J. Bansmann, M. Getzlaff, and G. Schönhense, Phys. Rev. Lett. **63**, 151 (1989).
[2] A. Kaminski, S. Rosenkranz, H. M. Fretwell, J. C. Campuzano, Z. Li, W. G. Cullen, H. You, C. G. Olson, C. M. Varma, and H. Höchst, Nature (London) **416**, 610 (2002).
[3] C. M. Varma, Phys. Rev. B **61**, R3804 (2000).
[4] Y. Liu, G. Bian, T. Miller, and T.-C. Chiang, Phys. Rev. Lett. **107**, 166803 (2011).
[5] Y. H. Wang, D. Hsieh, D. Pilon, L. Fu, D. R. Gardner, Y. S. Lee, and N. Gedik, Phys. Rev. Lett. **107**, 207602 (2011).
[6] W. Jung, Y. Kim, B. Kim, Y. Koh, C. Kim, M. Matsunami, S.-i. Kimura, M. Arita, K. Shimada, J. H. Han, J. Kim, B. Cho, and C. Kim, Phys. Rev. B **84**, 245435 (2011).
[7] S. R. Park, J. Han, C. Kim, Y. Y. Koh, C. Kim, H. Lee, H. J. Choi, J. H. Han, K. D. Lee, N. J. Hur, M. Arita, K. Shimada, H. Namatame, and M. Taniguchi, Phys. Rev. Lett. **108**, 046805 (2012).
[8] B. Kim, C. H. Kim, P. Kim, W. Jung, Y. Kim, Y. Koh, M. Arita, K. Shimada, H. Namatame, M. Taniguchi, J. Yu, and C. Kim, Phys. Rev. B **85**, 195402 (2012).

[9] G. Bian, L. Zhang, Y. Liu, T. Miller, and T.-C. Chiang, Phys. Rev. Lett. **108**, 186403 (2012).
[10] J.-H. Park, C. H. Kim, J.-W. Rhim, and J. H. Han, Phys. Rev. B **85**, 195401 (2012).
[11] Y. Ishida, H. Kanto, A. Kikkawa, Y. Taguchi, Y. Ito, Y. Ota, K. Okazaki, W. Malaeb, M. Mulazzi, M. Okawa, S. Watanabe, C.-T. Chen, M. Kim, C. Bell, Y. Kozuka, H. Y. Hwang, Y. Tokura, and S. Shin, Phys. Rev. Lett. **107**, 077601 (2011).
[12] F. Vidal, M. Eddrief, B. R. Salles, I. Vobornik, E. Velez-Fort, G. Panaccione, and M. Marangolo, Phys. Rev. B **88**, 241410(R) (2013).
[13] M. R. Scholz, J. Sánchez-Barriga, J. Braun, D. Marchenko, A. Varykhalov, M. Lindroos, Y. J. Wang, H. Lin, A. Bansil, J. Minár, H. Ebert, A. Volykhov, L. V. Yashina, and O. Rader, Phys. Rev. Lett. **110**, 216801 (2013).
[14] M. Neupane, S. Basak, N. Alidoust, S.-Y. Xu, C. Liu, I. Belopolski, G. Bian, J. Xiong, H. Ji, S. Jia, S.-K. Mo, M. Bissen, M. Severson, H. Lin, N. P. Ong, T. Durakiewicz, R. J. Cava, A. Bansil, and M. Z. Hasan, Phys. Rev. B **88**, 165129 (2013).
[15] M. Mulazzi, G. Rossi, J. Braun, J. Minár, H. Ebert, G. Panaccione, I. Vobornik, and J. Fujii, Phys. Rev. B **79**, 165421 (2009).
[16] M. Ärrälä, J. Nieminen, J. Braun, H. Ebert, and M. Lindroos, Phys. Rev. B **88**, 195413 (2013).
[17] S. LaShell, B. A. McDougall, and E. Jensen, Phys. Rev. Lett. **77**, 3419 (1996).
[18] L. Petersen and P. Hedegård, Surf. Sci. **459**, 49 (2000).
[19] M. Hoesch, M. Muntwiler, V. N. Petrov, M. Hengsberger, L. Patthey, M. Shi, M. Falub, T. Greber, and J. Osterwalder, Phys. Rev. B **69**, 241401(R) (2004).
[20] http://www.openmx-square.org.
[21] T. Ozaki, Phys. Rev. B **67**, 155108 (2003).
[22] J. Henk, M. Hoesch, J. Osterwalder, A. Ernst, and P. Bruno, J. Phys.: Condens. Matter **16**, 7581 (2004).
[23] J. Henk, A. Ernst, and P. Bruno, Phys. Rev. B **68**, 165416 (2003).
[24] T. C. Hsieh, P. John, T. Miller, and T.-C. Chiang, Phys. Rev. B **35**, 3728 (1987).
[25] S. G. Louie, P. Thiry, R. Pinchaux, Y. Pétroff, D. Chandesris, and J. Lecante, Phys. Rev. Lett. **44**, 549 (1980).
[26] S. D. Kevan and R. H. Gaylord, Phys. Rev. B **36**, 5809 (1987).
[27] T. Miller, W. E. McMahon, and T.-C. Chiang, Phys. Rev. Lett. **77**, 1167 (1996).